Geophys. J. R. astr. Soc. (1969) **18,** 159–175.

A Study of the Effects of the Yellowknife Crustal Structure upon the *P* Coda of Teleseismic Events

H. S. Hasegawa

(Received 1969 February 19)

Summary

The short-period *P* codas of seven earthquakes and four underground nuclear events recorded in the Yellowknife region of the Canadian Shield are analysed both in the time and in the frequency domains. In the time domain, the application of a '*P*-detection' filter to the earthquake events facilitates the identification of several phases (*pP* and *sP*) in the first 25 s of the *P* coda. The application of this filter to two nuclear events (originating at the Nevada Test Site) assists in the separation and in the identification of the crustal reverberations at the respective sources. In the frequency domain studies, the application of the spectral ratio test to six earthquake events resulted in poor agreement between the theoretical and the experimental spectral ratio curves; closer agreement was obtained for the nuclear events. Since the earthquake events did not possess the appropriate type of waveform for the spectral ratio test, it is not possible, at this stage, to pass judgment as to whether or not the crustal layering at Yellowknife fulfills the requirements of Haskell's matrix theory.

Signal-generated-noise studies are based on the observation of *P*-generated *SH* and *SV* waves. Anomalous *P–SH* conversion is much less in this region than in the sedimentary basin of central Alberta. However, there are indications of appreciable anomalous *P–SV* conversion; the source is likely in the lower part of the crust and possibly in the upper part of the mantle at Yellowknife.

Introduction

Several investigators have studied the *P*-coda of teleseismic events recorded at Canadian seismograph stations in order to determine the relation between location and relative recording ability of that station. The spectral structure of short-period *P*-wavetrains and the transmission coefficients of the incident *P*-waves were investigated by Ichikawa & Basham (1965), who suggest that the different recording abilities of stations can be explained by a combination of the shallow crustal effects which modify the character of the signal and the local noise properties. The spectral behaviour of both long- and short-period body waves at four of the Canadian Arctic stations has been studied by Utsu (1966) and an approximate estimate of the thickness of the crust and the surficial layer is given.

An intensive study of the effect of the sediments in central Alberta upon the character of short-period *P*-codas has been carried out by Ellis & Basham (1968), using magnetic tape records. These authors find only limited agreement between averaged vertical–horizontal spectral ratio curves and the corresponding theoretical curves. Their conclusion is that this region does not fulfill the requirements of Haskell's theory of the spectral response of a layered crust owing to scattering and anomalous *P*–*S* conversions in the crust and upper mantle.

The purpose of the present study is to evaluate how local crustal conditions in a simple geologic environment affect the character of short-period teleseismic signals. The Yellowknife region of the Canadian Shield was selected because both the crustal refraction survey by Barr (personal communication) and the Yellowknife array studies by Weichert (personal communication) indicate that the crust in this region can be represented by a simple two-layered structure with little or no evidence for dipping layers. Recent evidence which supports the selection of this site for *P*-coda studies is the study of signal-generated noise (*P*-generated surface waves) across the Yellowknife array by Key (1968), who finds little scattering across the array and states that most of the *P*-coda is due to coherent multiple reflections in the horizontal layering beneath the station and/or to source reverberations. In addition, the high gain settings for the Yellowknife seismic vault instruments is indicative of the comparatively low microseismic noise level in this region.

Recording sites

The locations of the three recording sites are shown in Fig. 1. At Yellowknife the site was on one of the spare piers in the Dominion Observatory seismic vault. At Rae the site was on a stretch of bedrock about 50 ft from a beach. At Fort Providence, the concrete floor of a storage shed was used.

The crustal models for the three sites are shown in Table 1. The values for the Yellowknife and Rae model were taken from the crustal refraction survey of this area by Barr (personal communication). The shear wave velocity for layer 1, however, was calculated on the assumption that this layer is a Poisson solid ($V_s = V_p/\sqrt{3}$). For the Fort Providence model there are two layers superimposed on the above model. Douglas (1959) shows that there is a surficial layer of drift of about 50 m

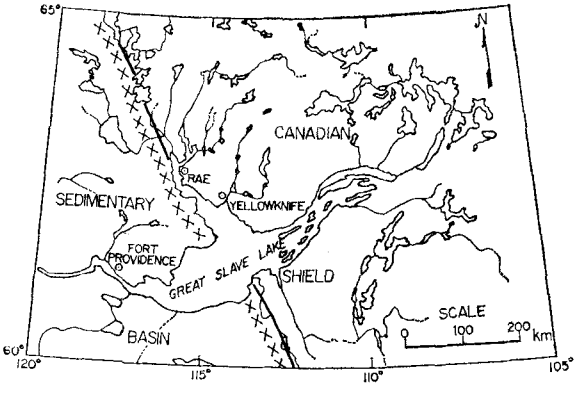

FIG. 1. Location of the three recording sites in the Yellowknife region of the Canadian Shield. The boundary between the Canadian Shield and the western Canada sedimentary basin is represented by the thick line segments with cross marks on the left.

Table 1

Seismic Models

Location	H	α	β	ρ	N
Yellowknife (YKC)	2·5	5·64	3·25	2·67	1
and Rae	32·0	6·15	3·69	2·84	2
	∞	8·18	4·71	3·32	3
Fort Providence	0·15	1·5	0·6	2·2	1
(FPD)	0·46	5·0	2·9	2·8	2
	2·5	5·64	3·25	2·67	3
	32·0	6·15	3·69	2·84	4
	∞	8·18	4·71	3·32	5

H = thickness (km).
α = compressional wave velocity (km s^{-1}).
β = shear wave velocity (km s^{-1}).
ρ = density (g cm^{-3}).
N = layer number.

in thickness overlying 460 m of Palaeozoic sediments of the Devonian and possibly older formations. The compressional wave velocity selected for the consolidated sediments is representative of the value obtained for the Devonian and Cambrian formations from well logs in central Alberta; velocities for the surficial layer of drift were taken from Press (1966).

Recordings were carried out on a continuous basis for about one month, commencing with the first week in July 1966.

Instrumentation

A block diagram of the portable seismographs used for this experiment is shown in Fig. 2. The corresponding response curves are shown in Fig. 3. The difference in response at the higher frequencies is due to the different responses of the amplifiers used; two systems have a photo tube-galvanometer amplifier with a natural period of 5 Hz; for the third system the upper cutoff is governed by the Butterworth filter setting, in this case 12·5 Hz. A detailed description of these portable seismographs is given by Bancroft & Basham (1967).

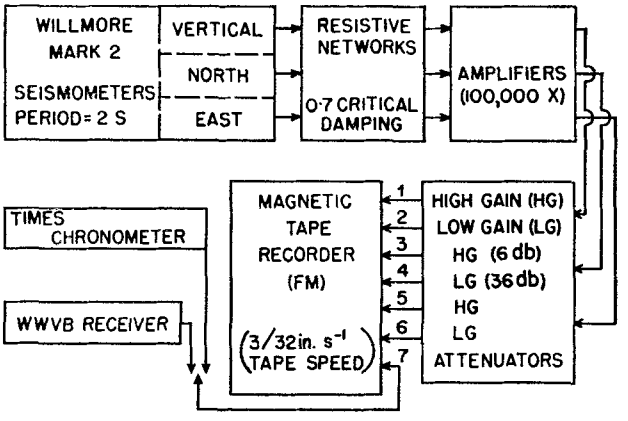

FIG. 2. Block diagram of the portable seismograph.

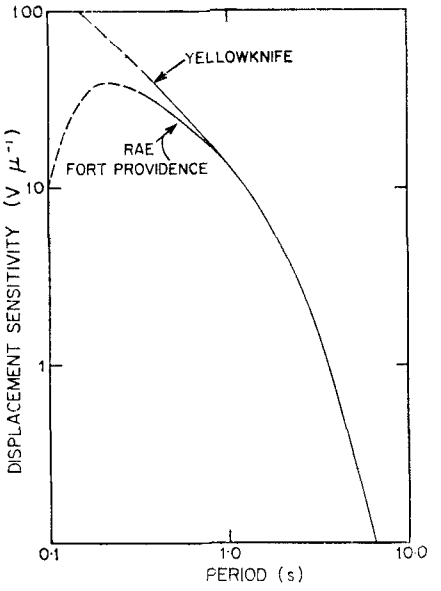

FIG. 3. Response curves of the portable seismograph.

Analogue-to-digital conversion

Conversion of the magnetic tape records from analogue (FM) to digital format was carried out at the Seismology Division of the Dominion Observatory in Ottawa. Selected events are played back on a Sanborn reproducer at ten times the recording speed; the output is fed into an analogue-to-digital converter which is in tandem with a DDP-124 computer. The sampling rate is 4 ms, which gives 25 samples per second of recording time, or a Nyquist frequency of 12·5 Hz, which is well above the frequency range of interest for *P*-wave studies. Digitization commenced about half a minute before the start of the earthquake and lasted for two min (real time). The digital data were then converted to a format suitable for the CDC-3100 Departmental computer and subsequent calculations were carried out on this computer.

Outline of data analysis

The short-period records of the *P*-coda of earthquakes and nuclear explosions are analysed in both the frequency and in the time domains. The criteria for selecting a record for analysis is that the signal-to-noise ratio be relatively large and that the maximum signal amplitude does not overload the tape. In the frequency domain, the spectral ratio method described by Phinney (1964) is used to determine to what extent the crustal layering around Yellowknife satisfies the requirements of Haskell's matrix theory (Haskell 1953). *A priori*, a comparison of the amplitude of the envelope of the transverse component with the vertical and the radial component envelopes is a good indication of the closeness of agreement to be expected between the theoretical and the experimental spectral ratios. In the time domain the '*P*-detection' (REMODE 3A) filter of Griffin (1966), which differentiates between *P*-type and *S*-type phases, is used to identify seismic phases such as *pP* and *sP* and, for the two nuclear events and time windows selected, to differentiate between source and local crustal structure effects.

The experimental spectrums were calculated by applying a rectangular data window to the *P*-coda and then Fourier-analysing this truncated record. A similar

data window was applied during the calculations of the theoretical crustal transfer functions using a method outlined by Leblanc (1967). The primary advantage in using this method is that, since both the theoretical and the experimental curves are equally distorted, the shape of the data window selected is not critical. For example, when this method is used, there is little to be gained by replacing the rectangular data window with a Hanning window for which the Fourier transform has very small side lobes. From the point of view of a weighing function which enhances the early part of the *P*-coda and suppresses the later arrivals (which contain signal-generated noise), the Hanning window is superior to the rectangular window when calculating the experimental curves. However, this advantage is offset by a decrease in 'resolution' when calculating the corresponding theoretical (truncated) transmission curves because the Hanning window would suppress the crustal reverberations which are the parts of the signal most characteristic of the crustal layering. The selection of the length of the data window, however, is still important; it should be long enough to include significant crustal reverberations associated with the initial *P*-pulse, but short enough to exclude later arriving phases such as *PP* and *PcP*, which arrive with incident angles different from those for the *P*-pulse.

Normalized transmission coefficients, $Up(f)$ and $Wp(f)$ for the horizontal and vertical components respectively, are first calculated by using the results derived by Haskell (1962). These calculations are carried out for the required crustal model, the appropriate angle of incidence (i) at the base of the crust, and over the frequency range of interest, which in this case is 0·025–4·5 Hz. Next the truncated transfer functions are calculated using two successive Fourier transformations. In the first step a time synthesis is performed; for the horizontal component the expression is

$$u(t) = \int_{0\cdot025}^{4\cdot5} Up(f)\, e^{-i2\pi ft}\, df. \tag{1}$$

Next, the time, Tc, taken for a P wave to travel upwards through the crust for a given incident angle, i, is calculated and a rectangular data window, Tw, is selected, which is equal in length to that used for the experimental spectral calculations. Finally, a Fourier transform gives

$$TUp(f) = \frac{1}{2\pi} \int_{Tc}^{Tc+Tw} u(t)\, e^{i2\pi ft}\, dt, \tag{2}$$

where $TUp(f)$ and $TWp(f)$ are the required truncated crustal transmission coefficients. A rectangular data window of 20 s is used and the angle, i, is calculated, using the Gutenberg A model; a time synthesis of the response of the Yellowknife crustal model to a spike input at the base for an incident angle, i, ranging from 1° to 89° indicates that crustal reverberations are relatively insignificant after 20 s from the first arrival.

The response of the '*P*-detection' filter, in this case the normalized or REMODE 3A filter, when plotted against the phase difference between two harmonic wave trains, is shown by Griffin (1966) to behave like a cosine curve with unit gain at zero phase difference and zero gain at ninety-degree phase difference. In this method the vertical (Z) and radial (R) traces are first rotated in the Z–R plane in order to partition the signal energy evenly between Z' and R', the rotated Z and R components. Next the cross-correlation, $C_{t,\,w}(\tau)$, for lag τ is calculated over a window w centred on time t as follows:

$$C_{t,\,w}(\tau) = \int_{t-w/2}^{t+w/2} Z'(t).R'(t+\tau)\, dt. \tag{3}$$

Then $C_t(\tau)$ is set equal to $C_t(-\tau)$, i.e. the positive lag correlations are set equal to the corresponding negative lag correlations. The resulting even function, $\phi_{t,w}(\tau)$ is then

$$\phi_{t,w}(\tau) = C_{t,w}(\tau). \tag{4}$$

In order that $\phi_{t,w}(\tau)$ be a P-detector, $\phi_{t,w}(0)$ is set equal to zero whenever $C_{t,w}(0)$ is negative, and conversely for a SV-detector. A time-varying normalization factor, σ_t^2, is introduced in order to make the filter response independent of signal amplitudes; this factor is

$$\sigma_t^2 = \left\{ \int_t^{t+w/2} (Z'(t))^2 \, dt \cdot \int_t^{t+w/2} (R'(t))^2 \, dt \right\}^{-\frac{1}{2}}. \tag{5}$$

Finally, the REMODE (3A) response is

$$(3A)\, \phi_{t,w}(\tau) = \sigma_t^2 . \phi_{t,w}(\tau), \tag{6}$$

which is dimensionless and depends more on the phase difference than on the amplitudes of Z' and R'. A convolution of Z' and R' with the expression in equation (6) gives the required filtered traces. A time window of 1·2 s (30 data points) and a maximum number of lags of 16 are used; these values are comparable to those used by Basham & Ellis (1969) in their study of the composition of short-period P-codas of teleseismic events recorded in the plains of central Alberta. These authors have applied a 'P-detection' polarization filter to 25 s of the record following the P onset in order to facilitate the detection of compressional phases such as the pP, sP, PcP and PKP phases; for events with pP phases visible at two stations, their measurements of pP–P times are accurate to about ± 1 s, allowing focal depth assignment to an accuracy of about ± 15 km.

A crustal deconvolution was carried out for one underground nuclear event. By removing the crustal response under the detectors, the effects of the crustal structure at the source and the mantle can be examined. The effects of the crust were removed by dividing the frequency spectrum of the record (with a 40-s rectangular window) by the corresponding theoretical crustal transfer function (for the Yellowknife model shown in Table 1) and then taking the inverse Fourier transform of the results.

Table 2

List of earthquakes

Event	Date	Time	Epicentre		Depth (km)	m
1	1966 July 5	02 : 21	52·2 N	178·4 W	66	4·9
2	1966 July 12	18 : 53	44·6 N	37·4 E	26	5·9
3	1966 July 13	08 : 20	12·6 N	87·7 W	61	5·3
4	1966 July 14	12 : 18	56·2 N	149·8 W	33	5·2
5	1966 July 17	08 : 46	61·9 N	152·0 W	103	4·8
6	1966 July 19	01 : 40	56·2 N	164·9 E	18	5·4
7	1966 July 21	18 : 30	17·8 S	178·6 W	591	5·6

Table 3

List of nuclear explosions

Event	Date	Time	Epicentre		m
BRONZE	1965 July 23	17 : 00	37·1 N	116·0 W	5·1
CHARTREUSE	1965 July 23	15 : 00	37·3 N	116·3 W	4·9
PIRANHA	1966 May 13	13 : 30	37·1 N	116·0 W	5·4
BOXCAR	1968 April 26	15 : 00	37·3 N	116·4 W	6·3

Table 4

Signal-to-noise (S/N) ratio and azimuth of earthquakes

Station	Event	S/N(0·25–2 Hz)	S/N(0·25–4 Hz)	Theoretical azimuth	Apparent azimuth
Yellowknife	1	4·77	4·87	282·9	285·4±0·7
Yellowknife	2	12·63	12·78	20·8	22·3±1·1
Yellowknife	3	1·66	1·79	146·8	137·0±1·9
Yellowknife	4	6·37	6·76	266·7	266·2±0·5
Yellowknife	6	2·53	2·46	298·9	305·3±1·2
Rae	3	0·15	0·18		
Rae	4	0·10	0·08		
Rae	6	0·38	0·32		
Fort Providence	2	4·10	2·50	18·4	15·5±1·3
Fort Providence	3	0·81	0·65	142·6	140·6±2·2
Fort Providence	4	9·6	6·4	267·1	268·5±0·5
Fort Providence	5	13·45	8·70	287·2	293·6±0·5
Fort Providence	6	2·68	2·03	298·3	300·5±0·9
Fort Providence	7	1·57	1·22	236·5	242·1±2·9

Results and discussion

Time and frequency domain studies were carried out on those events listed in Tables 2 and 3 for which the signal/noise (S/N) ratio were relatively high. No records from Rae were usable because of the extremely low S/N ratio (Table 4), which is due primarily to excessive wind noise.

The transverse components of the earthquake events shown in Fig. 4 do not show the marked build-up with time which is evident on the teleseismic records

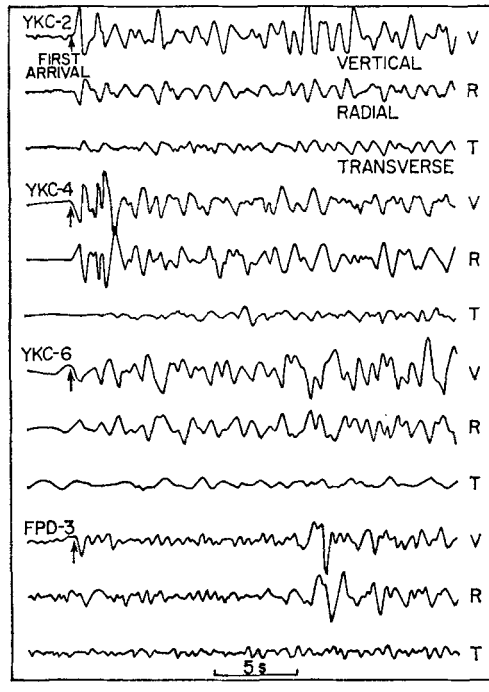

FIG. 4. Seismograms of the vertical, radial and transverse components of four earthquake events.

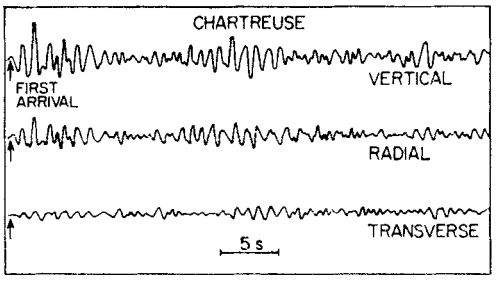

FIG. 5. Yellowknife seismic vault seismograms of an underground explosion originating at the Nevada Test Site.

taken on the sedimentary basin in central Alberta by Ellis & Basham. For a small, underground nuclear explosion originating at the Nevada Test Site, the corresponding transverse component (Fig. 5) also remains at a comparatively low level for the first 20 s. This lack of build-up of transverse energy and the fact that Key (1968) finds little *P*-generated surface waves across the Yellowknife area are, *a priori*, necessary conditions that the Yellowknife crustal layering must satisfy in order to fulfill the requirements of Haskell's theory of the spectral response of a layered crust.

Frequency domain studies

In general, there is poor agreement between the experimental and the theoretical spectral ratio curves for the earthquake events (see Figs 6–9). Some of the main factors contributing to the poor results are (a) the low S/N ratio for events 3, 6 and 7, (b) the relatively large secondary arrivals appearing in events 1, 3 and 4 (see Figs 13 and 14), (c) the slow build-up of energy in event 6. The closest fit was obtained

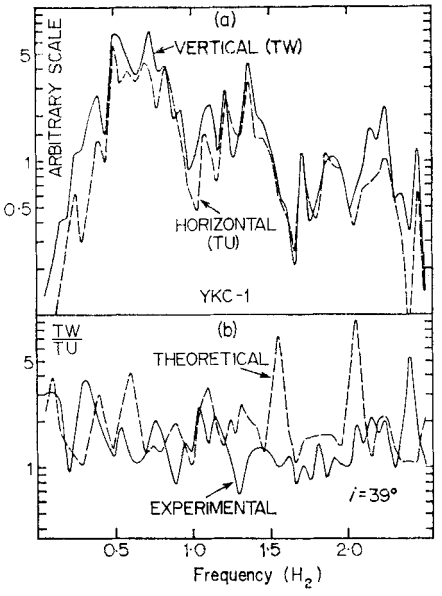

FIG. 6. (a) Spectral response of the vertical (TW) and radial horizontal (TU) components for event 1. (b) The corresponding experimental and theoretical spectral ratio curves. The angle of incidence, *i*, at the base of the crust is given.

for FPD-5; this event has a strong onset with an envelope which decreases monotonically and rapidly and, in addition, the S/N ratio is the largest of the earthquake events studied. In order to obtain a better fit between the theoretical and the experimental curves for FPD-5, the incident angle i (at the base of the crust) and the P and S wave velocities for the sedimentary layer (FPD layer 2 of Table 1) were perturbed. The epicentral distance for this event is 16° and for events closer than 20°, the calculated values for i are not reliable because the travel path of the signal is confined to the more or less complex upper mantle. The P-wave velocity for layer 2 is a representative value for the Devonian and Cambrian limestone layers in central Alberta (at a depth of close to 2 km) and consequently this velocity should be smaller at Fort Providence, where there is a layer of drift of only 0·05 km overlying this sedimentary layer. The effect of decreasing the P-wave velocity from 5 to 3 km s^{-1} is shown in parts (a), (b) and (c) of Fig. 10; the S-wave velocities are decreased in the same proportion in order that this layer remain a Poisson solid. As the velocities in layer 2 are decreased, there is an improvement in the correlation between the experimental and the theoretical curves in the frequency ranges 0·05–0·6 Hz and 1·3–1·9 Hz. With the exception of the peaks at 0·75 and 1·15 Hz, appearing in the theoretical curve in part (c), the correlation is fairly good. The effect upon the theoretical curves of perturbing i by $\pm 5°$ is shown in parts (d), (e) and (f) of Fig. 10; there does not appear to be any noticeable overall improvement.

A ' long period ' trend can be seen on the spectral ratio curves for the FPD events (see, for example, Fig. 10), but not on the YKC spectral ratio curves. This ' long period ' trend is generated by the thin surficial layers for which the spectral transfer

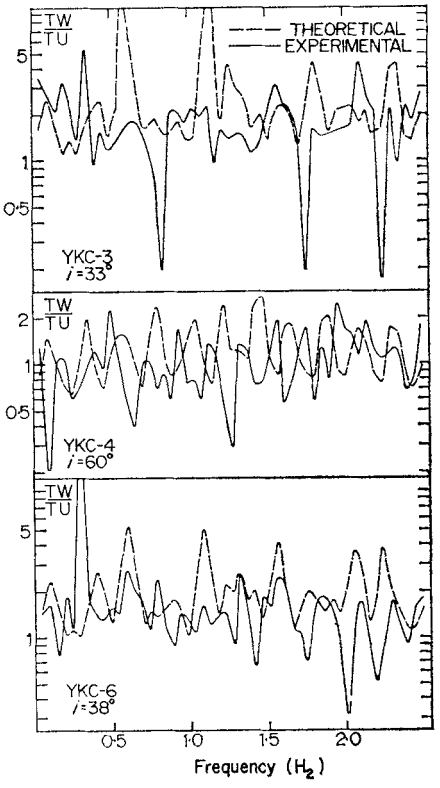

FIG. 7. Experimental and theoretical spectral ratio curves for three earthquake events recorded at Yellowknife (YKC).

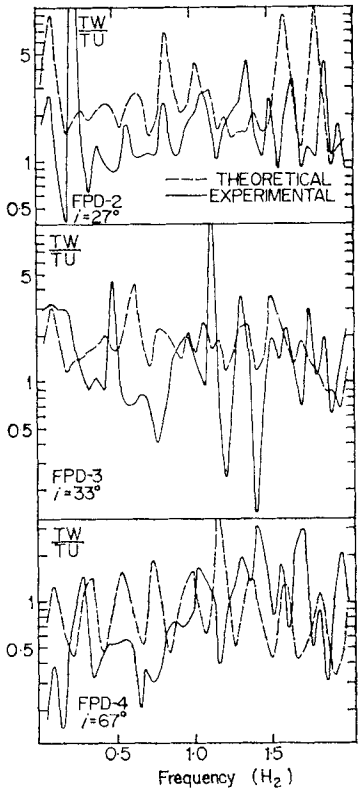

FIG. 8. Experimental and theoretical spectral ratio curves for three earthquake events recorded at Fort Providence (FPD).

ratio has widely spaced peaks (Phinney 1964; Hannon 1964). In so far as this 'long period' trend is concerned, the theoretical curve which gives the closest fit is shown in part (c) of Fig. 10 and this would indicate that the *P*-wave velocity for layer 2 is closer to 3 km s^{-1} than the originally selected value of 5 km s^{-1}.

The corresponding spectral ratio curves for the four nuclear events studied show better overall agreement. Closest agreement is obtained for the BRONZE event shown in Fig. 11. A value of 3·25 km s^{-1} for the shear wave velocity in the top layer was found to give the best fit; the other layer velocities were obtained from the refraction survey by Barr and consequently were not perturbed. Except for the phase reversal at 0·9 c/s, there is a fairly good correlation between the peaks and troughs of the observed curve and the corresponding features on the theoretical curve for the BRONZE event. The fit is not so close for the other three nuclear events shown in Fig. 11; a value of 3·50 km s^{-1} for the shear wave velocity in layer 1 was found to give a better fit for these three events. There appears to be a shift in phase between corresponding experimental and theoretical peaks at the low frequencies; a perturbation of the incident angle i by $\pm 3°$ did not improve the fit. One reason for the poor agreement is that, for an epicentral distance of only 25°, the *P*-coda may be a superposition of pulses travelling along several different routes in the upper mantle, and consequently arriving with different incident angles at the base of the Yellowknife crust; for example, there is a strong secondary arrival at close to 15 s after the first onset for the CHARTREUSE event. Even if this strong secondary event should happen to arrive at the base of the crust with an incident angle very close to that of the

initial pulse, the experimental (and consequently the theoretical) data window will have to be lengthened by an amount equal to the delay time of the second event. Since the Fast Fourier Transform program (which was used for all the Fourier analyses carried out in this study) requires that the number of data points must be 2^N where N is an integer, it is not feasible to vary the data window length to fit the record length and, consequently, the record length was held constant at 20 s.

Time domain studies

A comparison of the theoretical with the apparent azimuth for the earthquake events listed in Table 4 seems to indicate that, in general, there is no predominant dip in the crustal layering around Yellowknife. However, for events arriving from the northwest, the apparent azimuth is greater than the theoretical by an amount ranging from one to six degrees. For the Nevada Test Site events, an examination of the original Yellowknife seismograms shows that the onset of the transverse component is about 0·5 s later (on the average) than the P onset. This would indicate that the source for these early-arriving SH waves is within 4 km of the seismometers; it may well be the interface between layers 1 and 2 (see Table 1). If there were undulations in this boundary, then this could account for some of the observed P–SH converted phases.

The result of applying the 'P-detection', or P–D filter to two nuclear events of approximately the same amplitude and shot point are shown in Fig. 12. A time

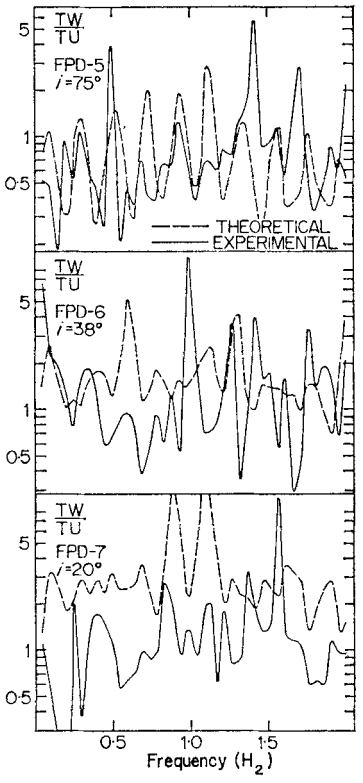

FIG. 9. Experimental and theoretical spectral ratio curves for three earthquake events recorded at Fort Providence.

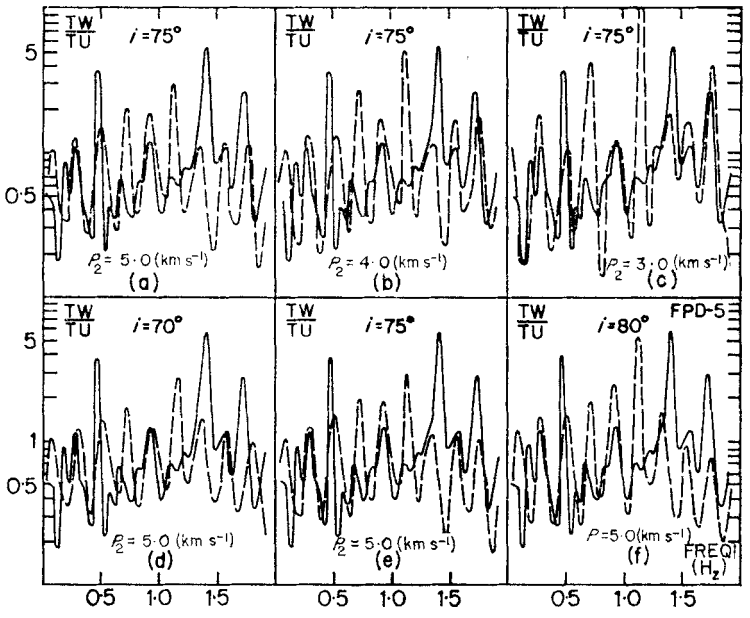

FIG. 10. Parts (a)–(c) show the variation in the theoretical (truncated) spectral ratio curves (dashed line segments) when the sedimentary layer velocities, P_2 and S_2, are varied; $i = 75°$ is the calculated incident angle.

Parts (d)–(f) show the variation in the theoretical spectral ratio curves when i is perturbed by $\pm 5°$ from the calculated value; the layer parameters are held constant.

The solid line curve in each part is the FPD-5 experimental spectral ratio curve; the epicentral distance is 16°.

synthesis by Hasegawa & Whitham (to be published) of the response of the Yellowknife crustal model to a plane compressional pulse incident at the base of the crust (at an angle $i = 41{\cdot}5°$) shows that crustal reverberations are about an order of magnitude smaller in amplitude than the (direct) first arrival. In addition, there is about a 4 s delay between the direct arrival and the first converted phase. Therefore, the early arriving *P*-type phases shown in the *P–D* filtered traces in Fig. 12 can be attributed almost entirely to crustal reverberations at the respective sources and differences in the respective records are indicative of the different crustal structure at the respective sources. Since the *P–D* filtered records show that the *P*-coda following the crustal reverberations at the source are predominantly of the *SV* type, this would indicate that there is appreciable anomalous *P-SV* conversion deep down in the crust and possibly in the upper mantle at Yellowknife. The *PP* (and also the *PPP* and *PcP*) phases arrive too late to appear on these traces and the *pP* phase is superimposed on the direct *P* wave and produces the relatively large second-arriving compressional peak.

Figs 13 and 14 illustrate the effect of applying the *P–D* filter to four earthquake events recorded at Yellowknife. The facility with which the *pP* phase can be detected and identified is manifest on some of these events; the *sP* phase can be identified on event 4. (The delay time for the *pP* and *sP* phases were obtained from Herrin (1968) and Jeffreys & Bullen (1958), respectively.) Other events such as *PP* and *PcP* arrive too late to appear on these 25-s records. For event 1, the two large maplitude phases arriving in between the weak *P* and *pP* phases are probably due

to complex source effects. For events 3 and 6, the pP amplitudes are greater than the corresponding initial P amplitudes; the orientations of the source P-radiation pattern which will produce this, plus other relative amplitude ratios for P/pP, are illustrated by Basham (1967).

In view of the fact that there is too much SV generation, as is shown in Fig. 12, a formal deconvolution using the Yellowknife crustal model (see Table 1) does not result in any significant modification in the P-coda. For example, Fig. 15 illustrates this point; the amplitudes are not to scale, the largest amplitude on each trace being

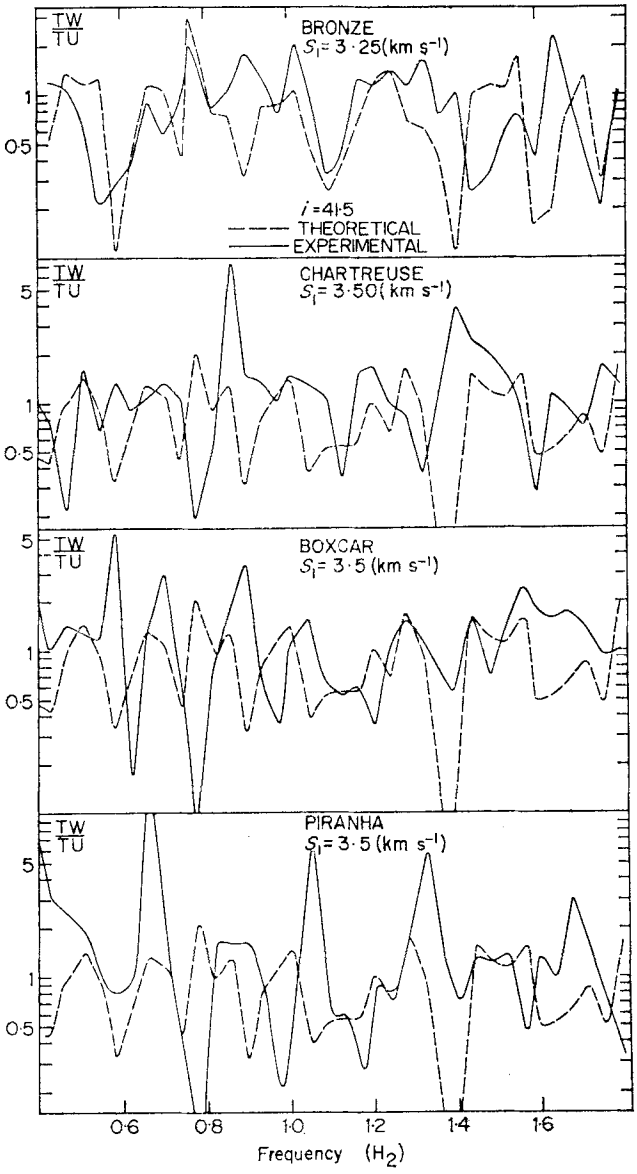

FIG. 11. Experimental and theoretical spectral ratio curves for four N.T.S. underground explosions recorded at Yellowknife. The shear wave velocity, S_1 (of layer 1 of the model shown in Table 1) which gives the best fit is shown above.

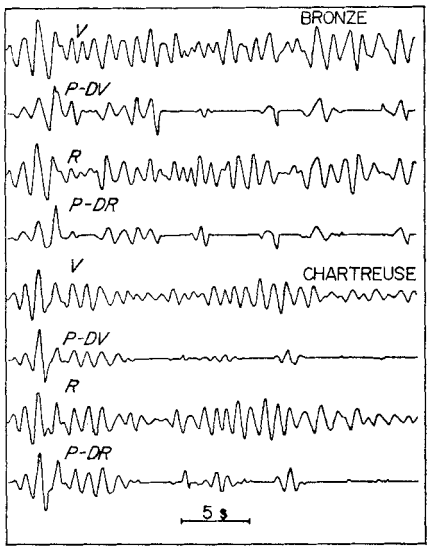

FIG. 12. ' P-detection ' (*P–D*) filters are applied to two N.T.S. events of magnitudes 5·1 (BRONZE) and 4·9 (CHARTREUSE). The amplitudes are not to scale. Pre-filtered with a 0·25–2·0 Hz bandpass (Lanczos) filter.

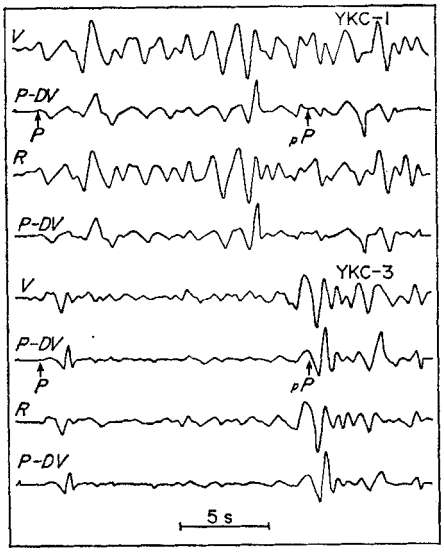

FIG. 13. ' P-detection ' (*P–D*) filters are applied to two earthquake events. The amplitudes are not to scale. Pre-filtered with a 0·25–2·0 Hz bandpass (Lanczos) filter.

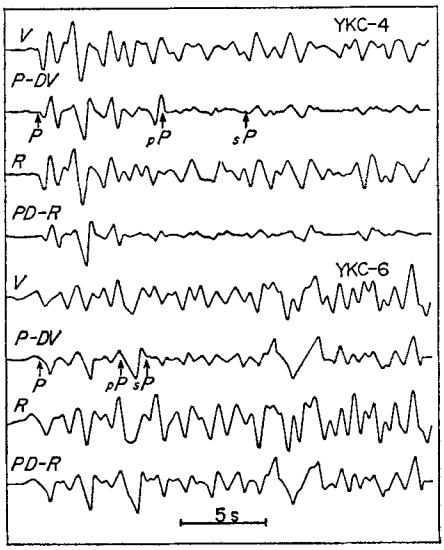

FIG. 14. ' P-detection ' (*P–D*) filters are applied to two earthquake events. The amplitudes are not to scale. Pre-filtered with a 0·25–2·0 Hz bandpass (Lanczos) filter.

set equal to each other and the shift in time of close to 5 s between the original and deconvolved record corresponds to the travel time of the initial *P*-wave upwards through the crust.

Conclusion

Time domain studies of the short-period *P*-codas of earthquake and nuclear events recorded in the Yellowknife region have facilitated the identification of seismic phases. For example, for earthquake events *pP* and *sP* phases have been identified; for underground nuclear events the crustal reverberations near the source are isolated from the signal-generated noise in the *P*-coda. However, frequency domain studies have not yielded any conclusive evidence concerning whether or not the crustal

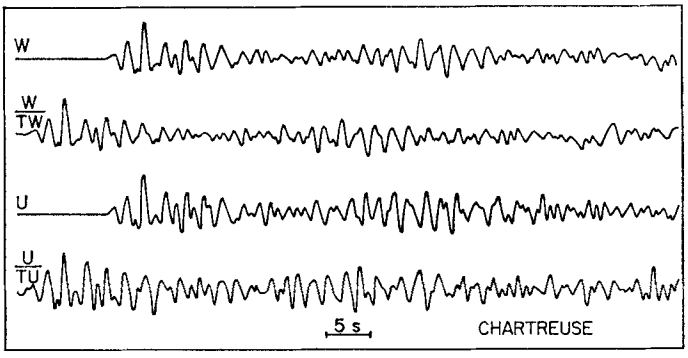

FIG. 15. Original (W and U) and deconvolved Yellowknife records of a N.T.S. event; the effect (TW and TU) of the Yellowknife crustal model has been removed in the deconvolved records. The amplitudes are not to scale.

layering at Yellowknife satisfies the requirements of Haskell's matrix theory. The agreement between the experimental and the theoretical spectral ratio curves is poor for the earthquake events but much better for the nuclear events.

A study of signal-generated noise at Yellowknife has produced some rather contradictory results. Anomalous *P*-generated *SH* phases have relatively small amplitudes and, in general, do not show a marked build-up with time; the early arriving phases are generated near the surface and the later arriving phases, at greater depths. However, an examination of the *P–D* filtered records indicates that there is appreciable anomalous *P*-generated *SV* phases deep down in the crust and possibly in the upper mantle at Yellowknife.

One of the factors contributing to the poor results obtained in the spectral ratio tests is that the earthquake events do not, in general, possess the appropriate waveform for this type of analysis. Consequently this question of whether or not the crustal layering at Yellowknife fulfills the requirements of Haskell's matrix theory needs further investigation. Favourable results will indicate that there is little signal-generated noise at Yellowknife; this viewpoint supports the observations by Key and also the present study on anomalous *P*-generated *SH* phases. However, unfavourable results will support the observation that there appears to be appreciable anomalous *P*-generated *SV* phases at Yellowknife.

Acknowledgments

The guidance and helpful comments of Dr K. Whitham throughout this project are gratefully acknowledged. Thanks are also due to his staff members who conducted the field programme in the summer of 1966 and who have assisted with various aspects of this study.

Seismology Division,
Dominion Observatory,
Ottawa.

1969 *February.*

References

Bancroft, A. M. & Basham, P. W., 1967. An *FM* magnetic tape recording seismograph, *Publs Dom. Obs.*, **35**, 199–217.

Basham, P. W., 1967. Time domain studies of short-period teleseismic *P* phases, Master of Science Thesis, University of British Columbia.

Basham, P. W. & Ellis, R. M., 1969. The composition of *P* codas using magnetic tape seismograms, *Bull. seism. Soc. Am.*, **59**, 475–488.

Douglas, R. J. W., 1959. Great Slave and Trout River map-areas, Northwest Territories, *Geol. Surv. Can.*, paper 58–11.

Ellis, R. M. & Basham, P. W., 1968. Crustal characteristics from short-period *P* waves, *Bull. seism. Soc. Am.*, **58**, 1681–1700.

Griffin, J. N., 1966. Applications and development of polarization (REMODE) filters, Seismic Data Laboratory Report No. 141, Earth Sciences Division, Teledyne Industries, Inc.

Hannon, W. J., 1964. An application of the Haskell-Thomson matrix method to the synthesis of the surface motion due to dilatational waves, *Bull. seism. Soc. Am.*, **54**, 2067–2079.

Hasegawa, H. S. & Whitham, K., 1969. Theoretical response of a seismograph at Yellowknife to an underground explosion at the Nevada Test Site, to be published.

Haskell, N. A., 1953. The dispersion of surface waves in multilayered media. *Bull. seism. Soc. Am.*, **43**, 17–34.

Haskell, N. A., 1962. Crustal reflection of plane *P* and *SV* waves, *J. geophys. Res.*, **67**, 4751–4767.

Herrin, E. (chairman), 1968. Seismological tables for *pP–P*, *Bull. seism. Soc. Am.*, **58**, 1232–1233.

Ichikawa, M. & Basham, P. W., 1965. Variations in short-periods records from Canadian seismograph stations, *Can. J. Earth Sci.*, **2**, 510–542.

Jeffreys, H. & Bullen, K. E., 1958. *Seismological Tables*, British Associations, Gray-Milne Trust, p. 49.

Key, F. A., 1968. Some observations and analyses of signal generated noise, *Geophys. J. R. astr. Soc.*, **15**, 377–392.

Leblanc, G. S. J., 1967. Truncated crustal transfer functions and fine crustal structure determination, *Bull. seism. Soc. Am.*, **57**, 719–733.

Phinney, R. A., 1964. Structure of the Earth's crust from spectral behaviour of long-period body waves, *J. geophys. Res.*, **69**, 2997–3017.

Press, F., 1966. *Seismic Velocities, Handbook of Physical Constants*, ed. by S. P. Clark, pp. 195–218, The Geological Society of America, Inc.

Utsu, T., 1966. Variations in spectra of *P* waves recorded at Canadian Arctic seismograph stations, *Can. J. Earth Sci.*, **3**, 597–621.